Cognitive Neurodynamics
https://doi.org/10.1007/s11571-024-10125-w

RESEARCH ARTICLE

Break-up and recovery of harmony between direct and indirect pathways in the basal ganglia: Huntington's disease and treatment

Sang-Yoon Kim[1] · Woochang Lim[1]

Received: 18 October 2023 / Revised: 21 April 2024 / Accepted: 7 May 2024

Abstract
The basal ganglia (BG) in the brain exhibit diverse functions for motor, cognition, and emotion. Such BG functions could be made via competitive harmony between the two competing pathways, direct pathway (DP) (facilitating movement) and indirect pathway (IP) (suppressing movement). As a result of break-up of harmony between DP and IP, there appear pathological states with disorder for movement, cognition, and psychiatry. In this paper, we are concerned about the Huntington's disease (HD), which is a genetic neurodegenerative disorder causing involuntary movement and severe cognitive and psychiatric symptoms. For the HD, the number of D2 SPNs (N_{D2}) is decreased due to degenerative loss, and hence, by decreasing x_{D2} (fraction of N_{D2}), we investigate break-up of harmony between DP and IP in terms of their competition degree $\mathcal{C}_d$, given by the ratio of strength of DP ($\mathcal{S}_{DP}$) to strength of IP ($\mathcal{S}_{IP}$) (i.e., $\mathcal{C}_d = \mathcal{S}_{DP}/\mathcal{S}_{IP}$). In the case of HD, the IP is under-active, in contrast to the case of Parkinson's disease with over-active IP, which results in increase in $\mathcal{C}_d$ (from the normal value). Thus, hyperkinetic dyskinesia such as chorea (involuntary jerky movement) occurs. We also investigate treatment of HD, based on optogenetics and GP ablation, by increasing strength of IP, resulting in recovery of harmony between DP and IP. Finally, we study effect of loss of healthy synapses of all the BG cells on HD. Due to loss of healthy synapses, disharmony between DP and IP increases, leading to worsen symptoms of the HD.

Keywords Basal ganglia · Huntington's disease · Direct pathway (DP) · Indirect pathways(IP) · Harmony between DP and IP · Competition degree · Optogenetics

Introduction

The basal ganglia (BG) (called the dark basement of the brain) are a group of subcortical deep-lying nuclei, receiving excitatory cortical input from most areas of cortex, and they provide inhibitory output to the thalamus and brainstem (Kandel et al. 1991; Squire et al. 2003; Bear et al. 2007; Luo 2016). The BG exhibit a variety of functions for motor control and regulation of cognitive and emotional processes (Kandel et al. 1991; Gurney et al. 2001a, b; Squire et al. 2003; Humphries et al. 2006; Bear et al. 2007; Humphries 2014; Mandali et al. 2015; Luo 2016; Humphries and Gurney 2021). Dysfunction in the BG is related to movement disorder [e.g., Parkinson's disease (PD) and Huntington's disease (HD)] and cognitive and psychiatric disorders (Kandel et al. 1991; Squire et al. 2003; Bear et al. 2007; Luo 2016).

In this paper, we are concerned about the HD. It is a rare hereditary neurodegenerative disease with severe symptoms for motor, cognition, and emotion (MacDonald et al. 1993; Bates 2005; Walker 2007; Ross and Tabrizi 2011; Paulsen et al. 2014; Bates et al. 2015; Rojas et al. 2022). As is well known, patients with HD show hyperkinetic dyskinesia such as chorea (involuntary jerky dance-like movement) as well as cognitive (e.g., dementia) and psychiatric (e.g,, depression and anxiety) disorders. In contrast, patients with PD show hypokinetic disorder such as slowed movement (bradykinesia) (Obeso et al. 2004, 2008; Guridi et al. 2012; Humphries et al. 2018; Armstrong and Okun 2020; Marino et al. 2020). Thus, if PD lies at one end of the spectrum of movement disorders in the BG, HD lies at the other end. We note that HD is caused by a mutated

✉ Woochang Lim
wclim@icn.re.kr

Sang-Yoon Kim
sykim@icn.re.kr

[1] Institute for Computational Neuroscience and Department of Science Education, Daegu National University of Education, Daegu 42411, Korea

Published online: 30 May 2024

huntingtin (HTT) gene on chromosome 4 (Gusella et al. 1983; MacDonald et al. 1993). As a result of mutation in HTT gene, the defective HTT gene has abnormal excessive repeats of a three-base (CAG) DNA sequence; in the mutant gene, the repeat occurs over and over again, from 40 times to more than 80. The greater the number of CAG repeats, the earlier the onset and severity of HD. This kind of trinucleotide repeat expansion results in production of abnormal HTT protein that accumulates, resulting in creation of toxic HTT protein aggregates damaging neurons (e.g., death of striatal cells in the BG). Thus, the primary pathological feature of HD is appearance of toxic HTT protein aggregates, causing the characteristic neurodegeneration seen in HD, in contrast to the case of PD where dopamine (DA) deficiency is a major cause.

In our recent work for the PD in the BG (Kim and Lim 2023), we made refinements on the spiking neural network (SNN) for the BG, based on the SNNs for the BG developed in previous works (Humphries et al. 2009a; Tomkins et al. 2014; Fountas and Shanahan 2017a); details on the SNN are given in Sec. II and Appendices in (Kim and Lim 2023). This SNN for the BG is based on anatomical and physiological data derived from rat-based works as follows. For the architecture of the BG SNN (e.g., number of BG cells and synaptic connection probabilities), we refer to the anatomical works (Oorschot 1996; Bar-Gad et al. 2003; Mailly et al. 2003; Sadek et al. 2007). For the intrinsic parameter values of single BG neurons, refer to the physiological properties of the BG neurons (Góngora-Alfaro et al. 1997; Richards et al. 1997; Bevan and Wilson 1999; Bevan et al. 2000, 2002; Hallworth et al. 2003; Wolf et al. 2005; Moyer et al. 2007; Gertler et al. 2008; Bugaysen et al. 2010; Liu et al. 2022). For the synaptic parameters (related to synaptic currents), we also refer to the physiological works (Park et al. 1982; Nakanishi et al. 1990; Fujimoto and Kita 1993; Götz et al. 1997; Dayan and Abbott 2001; Baufreton et al. 2005; Shen and Johnson 2006; Connelly et al. 2010; Ammari et al. 2011). Here, we use the rat-brain terminology throughout. The BG receive excitatory cortical input from most regions of cortex via the input nuclei [striatum and subthalamic nucleus (STN)] and project inhibitory output via the output nucleus [substantia nigra pars reticulata (SNr)], through the thalamus to the motor area of the cortex (Humphries et al. 2006; Mandali et al. 2015). We also note that, the principal input nucleus, striatum, is the primary recipient of DA, arising from the substantia nigra pars compacta (SNc). Within the striatum, spine projection neurons (SPNs), comprising up to 95 % of the whole striatal population, are the only primary output neurons (Bolam et al. 2006; Humphries et al. 2009b). There are two types of SPNs with D1 and D2 receptors for the DA. The DA modulates firing activity of the D1 and D2 SPNs in a different way (Humphries et al. 2009a; Tomkins et al. 2014; Fountas and Shanahan 2017a). In the early stage of HD, degenerative loss of D2 SPNs occurs due to mutation in the HTT gene, while DA level in the striatum is nearly normal (Reiner et al. 1988; Albin et al. 1992; Richfield et al. 1995; Han et al. 2010).

There are two competing pathways, direct pathway (DP) and indirect pathway (IP), in the BG (Albin et al. 1989; Alexander and Crutcher 1990; DeLong 1990; Kravitz et al. 2010). D1 SPNs in the striatum make direct inhibitory projection to the output nucleus, SNr, through DP, and then the thalamus becomes disinhibited. Consequently, movement facilitation occurs. In contrast, D2 SPNs are connected to the SNr through IP, crossing the intermediate control nucleus, GP (globus pallidus), and the STN. In the case of IP, the firing activity of the SNr becomes enhanced mainly because of excitatory input from the STN. As a result, firing activity of the thalamus becomes decreased, resulting in movement suppression.

Diverse functions of the BG could be made via "balance" of DP and IP. So far, a variety of subjects for the BG have been investigated in many computational works. Diverse neuron models were employed in the computational works; (a) artificial neurons of the leaky-integrator type (Gurney et al. 2001a, b; Humphries and Gurney 2021), (b) point neuron function using rate-coded output activation (Frank et al. 2001, 2004; Frank 2005), (c) leaky integrate-and-fire model (Humphries et al. 2006; Humphries 2014), (d) adaptive exponential integrate and fire model (Lindahl et al. 2013; Lindahl and Kotaleski 2016), (e) oscillatory model for local field potentials (Andres and Darbin 2018), (f) dendrite model (Mark et al. 2010), (g) firing rate model (Mulcahy et al. 2020), (h) multiple compartments model (Goodliffe et al. 2018), (i) Hodgkin-Huxley type neuron model (Rubin 2017; Wang et al. 2022; Yin et al. 2023), and (j) Izhikevich neuron model (Humphries et al. 2009a, b; Michmizos and Nikita 2011; Thibeault and Srinivasa 2013; Fountas and Shanahan 2014a, b; Tomkins et al. 2014; Mandali et al. 2015; Navarro-López et al. 2016; Celikok et al. 2016; Celikok and Sengör 2016; Fountas 2016; Kumaravelu et al. 2016; Fountas and Shanahan 2017a, b; Humphries et al. 2018; Sen-Bhattacharya et al. 2018; Cakir 2019; González-Redondo et al. 2020; Maith et al. 2021; Navarro-López et al. 2021; Yu et al. 2022).

But, no quantitative analysis for balance between DP and IP was made. As a first time, in our recent work (Kim and Lim 2023), we made quantitative analysis for competitive harmony (i.e., competition and cooperative interplay) between DP and IP by introducing their competition degree $\mathcal{C}_d$, given by the ratio of strength of DP ($\mathcal{S}_{DP}$) to strength of IP ($\mathcal{S}_{IP}$) (i.e., $\mathcal{C}_d = \mathcal{S}_{DP}/\mathcal{S}_{IP}$); $\mathcal{S}_{DP}$ ($\mathcal{S}_{IP}$) is given by the magnitude of the total time-averaged synaptic current into the output nucleus, SNr, through DP (IP).

In this paper, we take into consideration of degenerative loss of D2 SPNs for the HD; N_{D2} (number of D2 SPNs) = N^*_{D2} (normal value) x_{D2} [$1 > x_{D2}$ (fraction of number of D2 SPNs) ≥ 0] (Crossman 1987; Crossman et al. 1988; Reiner et al. 1988; Albin et al. 1992; Richfield et al. 1995; Han et al. 2010). By decreasing x_{D2} from 1, we investigate break-up of harmony between DP and IP for the HD by employing the competition degree $\mathcal{C}_d$ in the case of normal DA level ($\phi = 0.3$). Due to degenerative loss of D2 SPNs, IP becomes under-active (i.e., weakened), leading to increase in $\mathcal{C}_d$ from normal value. Thus, hyperkinetic dyskinesia such as chorea occurs, which is in contrast to the case of PD with reduced $\mathcal{C}_d$, causing hypokinetic disorder. Next, based on optogenetics (Kravitz et al. 2010; Tecuapetla et al. 2014), treatment of HD is also studied via recovery of harmony between DP and IP. Through activation of D2 SPN (STN) and deactivation of GP, IP becomes strengthened and thus harmony between DP and IP may be recovered. Finally, we investigate effect of loss of healthy synapses of all the BG cells on HD (Reiner et al. 1988; Klapstein et al. 2001; Cepeda et al. 2007; Milnerwood and Raymond 2010; Milnerwood et al. 2010; Plotkin, and Surmeier 2015).

This paper is organized as follows. In the main Sect. 2, in the SNN for the BG (Kim and Lim 2023), we make quantitative analysis of break-up and recovery of harmony between DP and IP for the HD. In the Supplementary Information (SI), brief description on the SNN for the BG is given. Finally, we give summary and discussion in Sect. 3.

Quantitative analysis of break-up and recovery of harmony between DP and IP for the HD

In this section, in the SNN for the BG considered in our prior work (Kim and Lim 2023), we quantitatively analyze competitive harmony (i.e., competition and cooperative interplay) between DP and IP for the HD in terms of the competition degree $\mathcal{C}_d$ between them, introduced in our previous work (Kim and Lim 2023). $\mathcal{C}_d$ is given by the ratio of strength of DP ($\mathcal{S}_{DP}$) to strength of IP ($\mathcal{S}_{IP}$) (i.e., $\mathcal{C}_d = \mathcal{S}_{DP}/\mathcal{S}_{IP}$).

As explained in the section of Introduction, we consider the SNN for the BG, based on anatomical and physiological data derived from rat-based studies. We note that, in the rat brain, the SNr is the only output nucleus of the BG, in contrast to the higher animals such as humans where both GPi (internal globus pallidus) and SNr are output nuclei. Figure 1 shows a box diagram for the SNN for the BG, consisting of D1/D2 SPNs, STN cells, GP cells, and SNr cells. As the single neuron model of the BG cells, we use the Izhikevich spiking neuron model (which is not only biologically plausible, but also computationally efficient) (Izhikevich 2003, 2004, 2007a, b). Blue colored cells and lines denote BG cells and synaptic connections affected by the DA. Both striatum and STN receive cortical inputs from most areas of the cortex. We model cortical inputs in terms of 1,000 independent Poisson spike trains with the same firing rate f. There are two pathways, DP (green) and IP (red). Inhibitory projection from the D1 SPNs to the output nucleus SNr is provided through the DP. In contrast, D2 SPNs are indirectly connected to the SNr through the IP, crossing the GP and the STN. Inhibitory output from the SNr to the thalamus/brainstem is controlled through competitive harmony between DP and IP (Kim and Lim 2023). In the SI, brief description on the SNN for the BG is given; for more details, refer to Sec. II in (Kim and Lim 2023).

Here, we consider the early stage of HD where neurodegerative loss of D2 SPNs occurs; N_{D2} (number of D2 SPNs) = N^*_{D2} (=1325; normal value) x_{D2} [$1 > x_{D2}$ (fraction of number of D2 SPNs) ≥ 0] (Crossman 1987; Crossman et al. 1988; Reiner et al. 1988; Albin et al. 1992; Richfield et al. 1995; Han et al. 2010). By decreasing x_{D2} from 1, we investigate break-up of harmony between DP and IP in both cases of tonic cortical input (3 Hz) in the resting state and phasic cortical input (10 Hz) in the phasically active state. In these cases, the IP becomes weakened, and thus $\mathcal{C}_d$

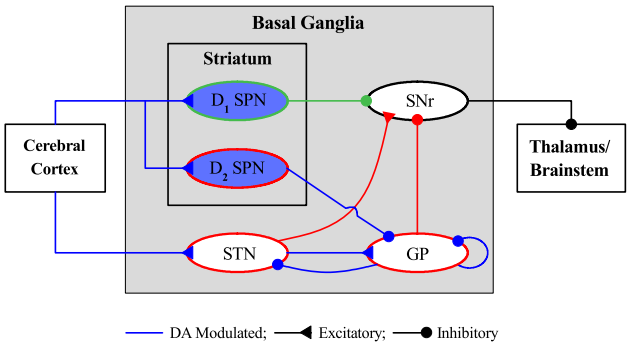

Fig. 1 Box diagram of our spiking neural network for the basal ganglia (BG). Excitatory and inhibitory connections are denoted by lines with triangles and circles, respectively, and dopamine-modulated cells and connections are represented in blue color. Striatum and STN (subthalamic nucleus), receiving the excitatory cortical input, are two input nuclei to the BG. In the striatum, there are two kinds of inhibitory spine projection neurons (SPNs); SPNs with the D1 receptors (D1 SPNs) and SPNs with D2 receptors (D2 SPNs). The D1 SPNs make direct inhibitory projection to the output nuclei SNr (substantia nigra pars reticulate) through the direct pathway (DP; green color). In contrast, the D2 SPNs are connected to the SNr through the indirect pathway (IP; red color) crossing the GP (globus pallidus) and the STN. The inhibitory output from the SNr to the thalamus/brainstem is controlled through competition between the DP and IP

becomes larger than normal ones. Consequently, involuntary jerky movement and abnormal hyperkinetic movement occur in the tonic and phasic cases, respectively. Next, we study treatment of HD through recovery of harmony between DP and IP. We strengthen the IP via activation of D2 SPNs and STN neurons and deactivation of GP neurons, based on optogenetics (Kravitz et al. 2010; Tecuapetla et al. 2014). Consequently, harmony between DP and IP becomes recovered, leading to normal movement. Finally, we also investigate the effect of loss of healthy synapses in the BG neurons on the HD.

Break-up of harmony between DP and IP for the HD

In the early stage of HD, we consider the case of normal DA level of $\phi_1 = \phi_2 = \phi = 0.3$ for the D1 and D2 SPNs. As explained above, cortical inputs are modeled in terms of 1,000 independent Poisson spike trains with firing rate f. We first consider the case of tonic cortical input with $f = 3$ Hz in the resting state (Bauswein et al. 1989; Turner and DeLong 2000; Zheng and Wilson 2002; Humphries et al. 2006, 2009b; Belforte et al. 2010; Reed et al. 2010; Lindahl et al. 2013; Fountas and Shanahan 2017a).

Population firing behavior of BG neurons could be well visualized in the raster plot of spikes, corresponding to a collection of spike trains of individual BG neurons. Figure 2a shows the raster plot of spikes for D1 SPNs, associated with DP (green color). In contrast to the case of D1 SPNs, degenerative loss of D2 SPNs occurs. With decreasing $x_{\rm D2}$ (i.e., fraction of number of D2 SPNs) from 1, we also get the raster plots of spikes of D2 SPNs [Fig. 2b1–b4], the STN neurons [Fig. 2d1–d4], and the GP neurons [Fig. 2e1–e4], related to the IP (red color) for $x_{\rm D2} = 1.0$, 0.8, 0.5, and 0.2.

As a collective quantity showing population behaviors, we employ an IPSR (instantaneous population spike rate) which may be obtained from the raster plot of spikes (Brunel and Wang 2003; Geisler et al. 2005; Brunel and Hakim 2008; Wang 2010; Kim and Lim 2014). Each spike in the raster plot is convoluted with a kernel function $K_h(t)$ to get a smooth estimate of IPSR $R_X(t)$ (Shimazaki and Shinomoto 2010):

$$R_X(t) = \frac{1}{N_X} \sum_{i=1}^{N_X} \sum_{s=1}^{n_i^{(X)}} K_h(t - t_{s,i}^{(X)}). \tag{1}$$

Here, N_X is the number of the neurons in the X population, and $t_{s,i}^{(X)}$ and $n_i^{(X)}$ are the sth spiking time and the total number of spikes for the ith neuron, respectively. We use a Gaussian kernel function of band width h:

$$K_h(t) = \frac{1}{\sqrt{2\pi}h} e^{-t^2/2h^2}, \quad -\infty < t < \infty, \tag{2}$$

where the band width h of $K_h(t)$ is 20 msec. The IPSRs $R_X(t)$ for $X =$ D1 (SPN), D2 (SPN), STN, GP, and SNr are also shown below their respective raster plots of spikes. Here, the case of $x_{\rm D2} = 1$ corresponds to the normal one without degenerative loss of D2 SPNs. With decreasing $x_{\rm D2}$ from 1, the population firing activities of the D2 SPNs, the STN neurons, and the GP neurons, associated with IP (red), are changed, while that of the D1 SPN, related to DP (green), is unchanged.

We also study the population-averaged mean firing rate (MFR) of the neurons $\langle f_i^{(X)} \rangle$ in the X population [$X =$ D1 (SPN), D2 (SPN), STN, and GP]; $f_i^{(X)}$ is the MFR of the ith neuron in the X population, and $\langle \cdots \rangle$ represents a population average over all the neurons. For the D1 and D2 SPNs, $\langle f_i^{(\rm D1)} \rangle = 1.03$ Hz and $\langle f_i^{(\rm D2)} \rangle = 0.97$ Hz, independently of $x_{\rm D2}$, because there is no change in cortical inputs to the D1/D2 SPNs; see Fig. 2c for the D2 SPNs. As $x_{\rm D2}$ is decreased from 1, $\langle f_i^{(\rm GP)} \rangle$ of the GP neurons is increased from 29.9 to 38.8 Hz, due to decrease in inhibitory projection from the D2 SPNs, as shown in Fig. 2g. In contrast, because of increased inhibitory projection from the GP, $\langle f_i^{(\rm STN)} \rangle$ of the STN neurons is decreased from 9.9 to 6.5 Hz [see Fig. 2f].

We note that, there are two types of synaptic currents into the (output) SNr neurons, I_{DP} and I_{IP}, via DP (green) and IP (red) in Fig. 1, respectively. The DP current, $I_{DP}(t)$, is just the (inhibitory) synaptic current from the D1 SPNs to the SNr neurons:

$$I_{DP}(t) = -I_{syn}^{(\rm SNr,D1)}(t). \tag{3}$$

There is no change in $I_{DP}(t)$, independently of $x_{\rm D2}$.

The IP current, $I_{IP}(t)$, is composed of the excitatory component, $I_{IP}^{(E)}(t)$, and the inhibitory component, $I_{IP}^{(I)}(t)$:

$$I_{IP}(t) = I_{IP}^{(E)}(t) + I_{IP}^{(I)}(t). \tag{4}$$

Here, $I_{IP}^{(E)}(t)$ [$I_{IP}^{(I)}(t)$] is just the synaptic current from the STN (GP) to the SNr:

$$\begin{aligned} I_{IP}^{(E)}(t) &= -I_{syn}^{(\rm SNr,STN)}(t) \quad \text{and} \\ I_{IP}^{(I)}(t) &= -I_{syn}^{(\rm SNr,GP)}(t). \end{aligned} \tag{5}$$

Unlike the case of $I_{DP}(t)$, with decreasing $x_{\rm D2}$ from 1, $I_{IP}(t)$ becomes decreased due to decrease in $I_{IP}^{(E)}(t)$ and increase in $|I_{IP}^{(I)}(t)|$ ($|\cdots|$: absolute magnitude).

Firing activity of the (output) SNr neurons is determined through competition between $I_{DP}(t)$ (DP current) and $I_{IP}(t)$ (IP current) into the SNr. The strengths of DP and IP, $\mathcal{S}_{DP}$

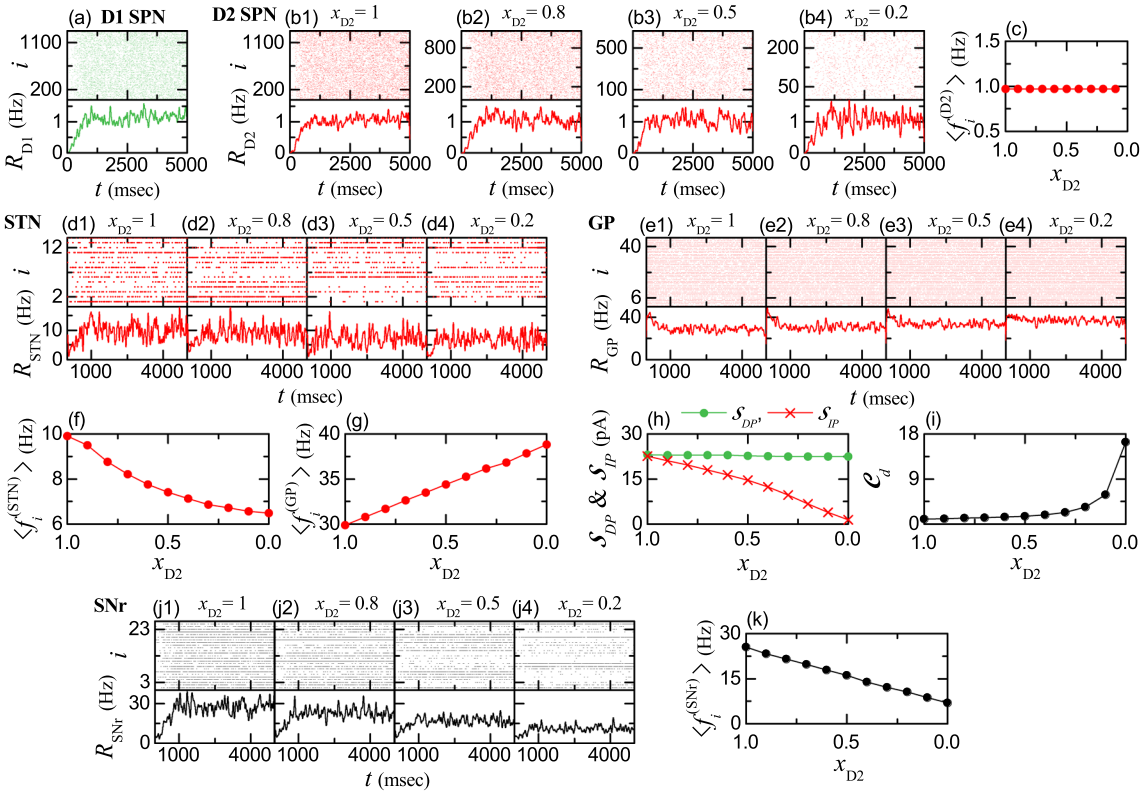

Fig. 2 Involuntary jerky movement due to degenerative loss of D2 SPNs in the tonic pathological state for the tonic cortical input (3 Hz) in the resting state. Colors: parts, related to DP (green), while parts, associated with IP (red). **a** Raster plot of spikes and IPSR (instantaneous population spike rate) $R_{D1}(t)$ of D1 SPNs. Raster plots of spikes and IPSRs $R_{D2}(t)$ of D2 SPNs for **b1** x_{D2} = 1.0, **b2** 0.8, **b3** 0.5, and **b4** 0.2. **c** Plot of population-averaged MFR (mean firing rate) $\langle f_i^{(D2)} \rangle$ of D2 SPNs versus x_{D2}. Raster plots of spikes and IPSRs $R_{STN}(t)$ of STN neurons for **d1** x_{D2} = 1.0, **d2** 0.8, **d3** 0.5, and **d4** 0.2. Raster plots of spikes and IPSRs $R_{GP}(t)$ of GP neurons for **e1** x_{D2} = 1.0, **e2** 0.8, **e3** 0.5, and **e4** 0.2. Plots of population-averaged MFRs of (f) STN neurons $\langle f_i^{(STN)} \rangle$ and **g** GP neurons $\langle f_i^{(GP)} \rangle$ versus x_{D2}. **h** Plots of strengths of DP $\mathcal{S}_{DP}$ and IP $\mathcal{S}_{IP}$ versus x_{D2}. **i** Plot of the competition degree $\mathcal{C}_d$ versus x_{D2}. Raster plot of spikes and IPSR $R_{SNr}(t)$ of SNr neurons for **j1** x_{D2} =1, **j2** 0.8, **j3** 0.5, and **j4** 0.2. **k** Plot of population-averaged MFR $\langle f_i^{(SNr)} \rangle$ of SNr neurons versus x_{D2}

and $\mathcal{S}_{IP}$, are given by the magnitudes of their respective time-averaged synaptic currents:

$$\mathcal{S}_{DP} = |\overline{I_{DP}(t)}| \quad \text{and} \quad \mathcal{S}_{IP} = |\overline{I_{IP}(t)}|, \tag{6}$$

where the overline denotes the time averaging and $|\cdots|$ represents the absolute magnitude. Then, the competition degree $\mathcal{C}_d$ between DP and IP (given by the ratio of $\mathcal{S}_{DP}$ to $\mathcal{S}_{IP}$) was introduced in (Kim and Lim 2023):

$$\mathcal{C}_d = \frac{\mathcal{S}_{DP}}{\mathcal{S}_{IP}}. \tag{7}$$

For $x_{D2} = 1$ (without degenerative loss of D2 SPNs), $\mathcal{S}_{DP}$ = 23.1 and $\mathcal{S}_{IP}$ = 23.4, and hence DP and IP become nearly balanced (i.e., $\mathcal{C}_d = 0.99$). In this non-degenerative case, the SNr neurons fire very actively with $\langle f_i^{(SNr)} \rangle = 25.5$ Hz. Due to strong inhibitory projection from the SNr, the thalamic cells become silent, resulting in no movement (i.e., the BG door to the thalamus is locked in the normal tonic default state).

But, with decreasing x_{D2} from 1 (degenerative case), as shown in Fig. 2h, $\mathcal{S}_{IP}$ is rapidly decreased from 23.4 to 1.4, while there is no change in $\mathcal{S}_{DP}$ (= 23.1). In this way, IP for the HD becomes weakened. Thus, as x_{D2} is decreased from 1, the competition degree $\mathcal{C}_d$ between DP and IP is found to increase from 0.99 to 16.5 [see Fig. 2i]. Thus, balance between DP and IP becomes broken up in the degenerative tonic case.

Figure 2j1–j4 show raster plots of spikes and IPSRs $R_{SNr}(t)$ of the (output) SNr neurons for x_{D2} = 1.0, 0.8, 0.5, and 0.2, respectively. We note that, firing activity of the SNr neurons becomes reduced with decreasing x_{D2} because of weakened IP. As a result of decrease in $\mathcal{S}_{IP}$ (strength of IP), the population-averaged MFR $\langle f_i^{(SNr)} \rangle$ is found to decrease from 25.5 to 6.9 Hz with decreasing x_{D2} from 1, as shown in Fig. 2k. Thus, the BG gate to the thalamus becomes opened even in the case of tonic cortical input (3 Hz) in the resting state via break-up of balance between DP and IP. Consequently, a tonic pathological state with

involuntary jerky movement occurs, in contrast to the tonic default state without movement.

Next, we consider the case of phasic cortical input (10 Hz) in the phasically active state (Bauswein et al. 1989; Turner and DeLong 2000; Zheng and Wilson 2002; Humphries et al. 2006, 2009b; Belforte et al. 2010; Reed et al. 2010; Lindahl et al. 2013; Fountas and Shanahan 2017a), which is shown in Fig. 3. Population firing behavior of D1 SPNs, associated with DP (green color), is shown in their raster plot of spikes and the IPSR $R_{D1}(t)$ in Fig. 3a. In comparison to the tonic case with the population-averaged MFR $\langle f_i^{(D1)} \rangle$ = 1.03 Hz in Fig. 2a, firing activity of the D1 SPNs become very active with $\langle f_i^{(D1)} \rangle$ = 30.7 Hz, independently of x_{D2}.

But, due to degenerative loss of D2 SPNs, population firing activities of the D2 SPNs, the STN neurons, and the GP neurons [related to the IP (red color)] are changed with decreasing x_{D2}, as shown in their raster plots of spikes and IPSRs in Fig. 3. The population-averaged MFRs of the D2 SPNs, the STN neurons, and the GP neurons are also shown in Fig. 3c, f, and g, respectively. For the D2 SPNs, $\langle f_i^{(D2)} \rangle$ = 24.1 Hz [much larger than that (0.97 Hz) in the tonic case], independently of x_{D2}, because there is no change in cortical input to the D2 SPNs. As a result of decreased inhibitory projection from the D2 SPNs, $\langle f_i^{(GP)} \rangle$ of the GP neurons is rapidly increased from 7.3 to 66.1 Hz with decreasing x_{D2} from 1; the increasing rate is higher than the tonic case. On the other hand, due to increase in inhibitory projection from the GP, $\langle f_i^{(STN)} \rangle$ of the STN neurons decreases from 39.8 to 17.6 Hz; the decreasing rate is also larger than that in the tonic case.

We consider the case of $x_{D2} = 1$ without degeneration. In this non-degenerative case, $\mathcal{S}_{DP}$ = 2309.7 and $\mathcal{S}_{IP}$ = 815.6. Thus, the competition degree becomes $\mathcal{C}_d = 2.82$ [i.e., $\mathcal{S}_{DP}$ (strength of DP) is 2.82 times larger than $\mathcal{S}_{IP}$ (strength of IP)]. In this case, $\langle f_i^{(SNr)} \rangle$ of the (output) SNr neurons are decreased to 5.5 Hz (cf., in the tonic case, 25.5 Hz). Consequently, the BG door to the thalamus becomes

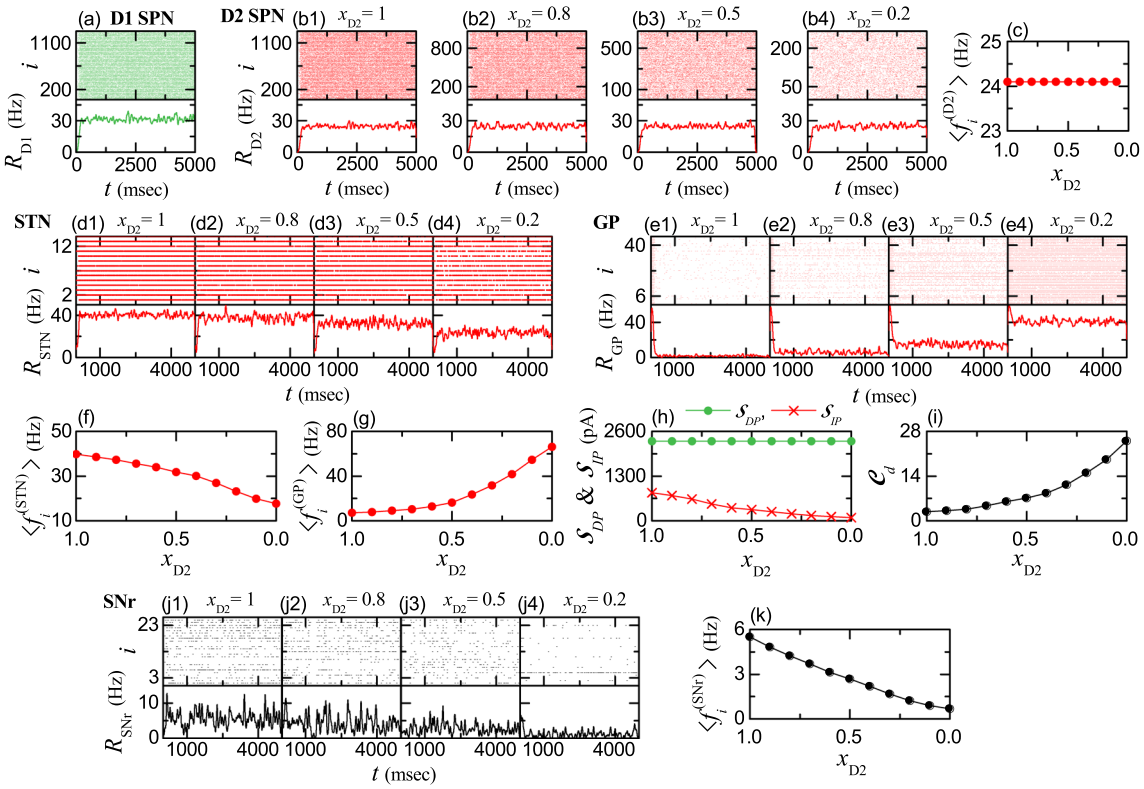

Fig. 3 Abnormal hyperkinetic movement due to degenerative loss of D2 SPNs in the phasic pathological state for the phasic cortical input (10 Hz) in the phasically-active state. Colors: parts, related to DP (green), while parts, associated with IP (red). **a** Raster plot of spikes and IPSR (instantaneous population spike rate) $R_{D1}(t)$ of D1 SPNs. Raster plots of spikes and IPSRs $R_{D2}(t)$ of D2 SPNs for **b1** x_{D2} = 1.0, **b2** 0.8, **b3** 0.5, and **b4** 0.2. **c** Plot of population-averaged MFR (mean firing rate) $\langle f_i^{(D2)} \rangle$ of D2 SPNs versus x_{D2}. Raster plots of spikes and IPSRs $R_{STN}(t)$ of STN neurons for **d1** x_{D2} = 1.0, **d2** 0.8, **d3** 0.5, and **d4** 0.2. Raster plots of spikes and IPSRs $R_{GP}(t)$ of GP neurons for **e1** x_{D2} = 1.0, **e2** 0.8, **e3** 0.5, and **e4** 0.2. Plots of population-averaged MFRs of **f** STN neurons $\langle f_i^{(STN)} \rangle$ and **g** GP neurons $\langle f_i^{(GP)} \rangle$ versus x_{D2}. **h** Plots of strengths of DP $\mathcal{S}_{DP}$ and IP $\mathcal{S}_{IP}$ versus x_{D2}. **i** Plot of the competition degree $\mathcal{C}_d$ versus x_{D2}. Raster plot of spikes and IPSR $R_{SNr}(t)$ of SNr neurons for **j1** x_{D2} =1, **j2** 0.8, **j3** 0.5, and **j4** 0.2. **k** Plot of population-averaged MFR $\langle f_i^{(SNr)} \rangle$ of SNr neurons versus x_{D2}

opened, leading to normal movement. This phasic healthy state with $\mathcal{C}_d = 2.82$ is in contrast to the tonic healthy state with $\mathcal{C}_d \simeq 1.0$ resulting in no movement.

However, as x_{D2} is decreased from 1 (degenerative case), $\mathcal{S}_{IP}$ is rapidly decreased from 815.6 to 92.3, while there is no change in $\mathcal{S}_{DP}$ (= 2309.7) [see Fig. 3h]. Thus, IP becomes rapidly weakened. Due to such under-activity of IP, the competition degree $\mathcal{C}_d$ increases from 2.82 (healthy state) to 25.0, as shown in Fig. 3i. Consequently, harmony between DP and IP becomes broken up in the degenerative case with $x_{\mathrm{D2}} < 1$, and then a phasic pathological state with abnormal hyperkinetic movement appears, in contrast to the phasic healthy state with normal movement.

Raster plots of spikes and IPSRs $R_{\mathrm{SNr}}(t)$ of the (output) SNr neurons for x_{D2} = 1.0, 0.8, 0.5, and 0.2 are shown in Fig. 3j1–j4, respectively. Due to under-activity of IP, firing activity of the SNr neurons becomes decreased with decreasing x_{D2} from 1. Due to decreased $\mathcal{S}_{IP}$ (strength of IP), the population-averaged MFR $\langle f_i^{(\mathrm{SNr})} \rangle$ decreases from 5.5 (healthy state) to 0.7 Hz with decreasing x_{D2} from 1 [see Fig. 3k]. In this phasic pathological state with $\mathcal{C}_d > 2.82$ (where harmony between DP and IP is broken up), abnormal hyperkinetic movement disorder occurs, in contrast to the normal movement for the phasic healthy state with $\mathcal{C}_d = 2.82$ (where there is harmony between DP and IP).

To sum up the above results briefly, it is shown that, for the HD, pathological states (where harmony between DP and IP is broken up) appear due to degenerative loss of D2 SPNs in the cases of both tonic and phasic cortical inputs. On the other hand, for the PD, pathological states appear because of DA deficiency (Obeso et al. 2004, 2008; Guridi et al. 2012; Humphries et al. 2018; Armstrong and Okun 2020; Marino et al. 2020; Kim and Lim 2023). In the case of HD, IP is under-active, in contrast to the case of PD with over-active IP. Thus, patients with HD exhibit abnormal hyperkinetic movement disorder, while patients with PD show abnormal hypokinetic movement disorder. Consequently, HD lies at one end of the spectrum of movement disorders in the BG, while PD lies at the other end.

Treatment of HD via recovery of harmony between DP and IP

For the pathological state in the HD, IP is under-active due to degenerative loss of D2 SPNs, in comparison to the healthy state. Thus, harmony between DP and IP is broken up (i.e. occurrence of disharmony between DP and IP), leading to abnormal hyperkinetic movement disorder. Here, based on optogenetics (Kravitz et al. 2010; Tecuapetla et al. 2014), we investigate treatment of the pathological state with enhanced competition degree $\mathcal{C}_d$ (than the normal one for the healthy state) in both cases of tonic and phasic cortical inputs via recovery of harmony between DP and IP.

Optogenetics is a control technique for the activity of target cells in living organisms by combining optics and genetics. The target cells are genetically modified to express opsins (light-sensitive proteins) (i.e., fusion of the opsins into the target cells). When the opsins are activated by the light stimulation with specific wavelengths, variation in the intrinsic ionic currents of the cells in the target population X, $\Delta I_{ion}^{(X)}$, takes place (Kravitz et al. 2010; Tecuapetla et al. 2014). If $\Delta I_{ion}^{(X)}$ is positive (negative), firing activity of the target cells is increased (decreased), resulting in their activation (deactivation). Such activation and deactivation of the target cells was studied in our recent work (Kim and Lim 2023). As discussed in (Kim and Lim 2023), we simulate the effect of optogenetics by adding $\Delta I_{ion}^{(X)}$ in Eq. (A1) in Appendix A in (Kim and Lim 2023), in addition to the current, $I_i^{(X)}$, into the target X population. With increasing the intensity of light stimulation, the magnitude of $\Delta I_{ion}^{(X)}$ also increases.

We first consider tonic pathological states with enhanced competition degree $\mathcal{C}_d$ [larger than that (1) for the tonic healthy state (with balanced DP and IP)], occurring due to degenerative loss of D2 SPNs, in the case of tonic cortical input (3 Hz) (see Fig. 2). As an example, we consider the tonic pathological case of $x_{\mathrm{D2}} = 0.5$ with $\mathcal{C}_d = 1.53$. In this pathological case, IP is under-active in comparison to the tonic healthy case (with balanced DP and IP); firing activity of D2 SPNs is under-active, leading to over-activity of GP neurons, which then results in under-activity of the STN neurons. Hence, for recovery of balance between DP and IP, we try to strengthen the IP via activation of D2 SPNs and STN neurons and deactivation of GP neurons.

We first strengthen the IP through activation of the target (under-active) D2 SPNs. Figure 4a1 shows plots of $\mathcal{S}_{IP}$ (strength of IP) and $\mathcal{S}_{DP}$ (strength of DP) versus $\Delta I_{ion}^{(\mathrm{D2})}$. As $\Delta I_{ion}^{(\mathrm{D2})}$ is increased from 0, $\mathcal{S}_{IP}$ (red) increases from 15.1, while $\mathcal{S}_{DP}$ (green) remains unchanged (i.e., 23.1). As a result of increase in $\mathcal{S}_{IP}$, the competition degree $\mathcal{C}_d$ between DP and IP is found to decrease from 1.53 [Fig. 4a2]. Also, the population-averaged MFR of the output SNr neurons, $\langle f_i^{(\mathrm{SNr})} \rangle$, is found to increase from 16.1 Hz [Fig. 4a3].

We note that, as $\Delta I_{ion}^{(\mathrm{D2})}$ passes a threshold $\Delta I_{ion}^{(\mathrm{D2})*}$ (= 262 pA), $\mathcal{C}_d = \mathcal{C}_d^*$ (= 1.0) and $\langle f_i^{(\mathrm{SNr})} \rangle = \langle f_i^{(\mathrm{SNr})*} \rangle$ (= 25.5 Hz); $\mathcal{C}_d^*$ and $\langle f_i^{(\mathrm{SNr})*} \rangle$ are those for the tonic healthy state, and they are represented by the horizontal dashed lines in Fig. 4a2 and a3. Thus, for $x_{\mathrm{D2}} = 0.5$, the pathological state

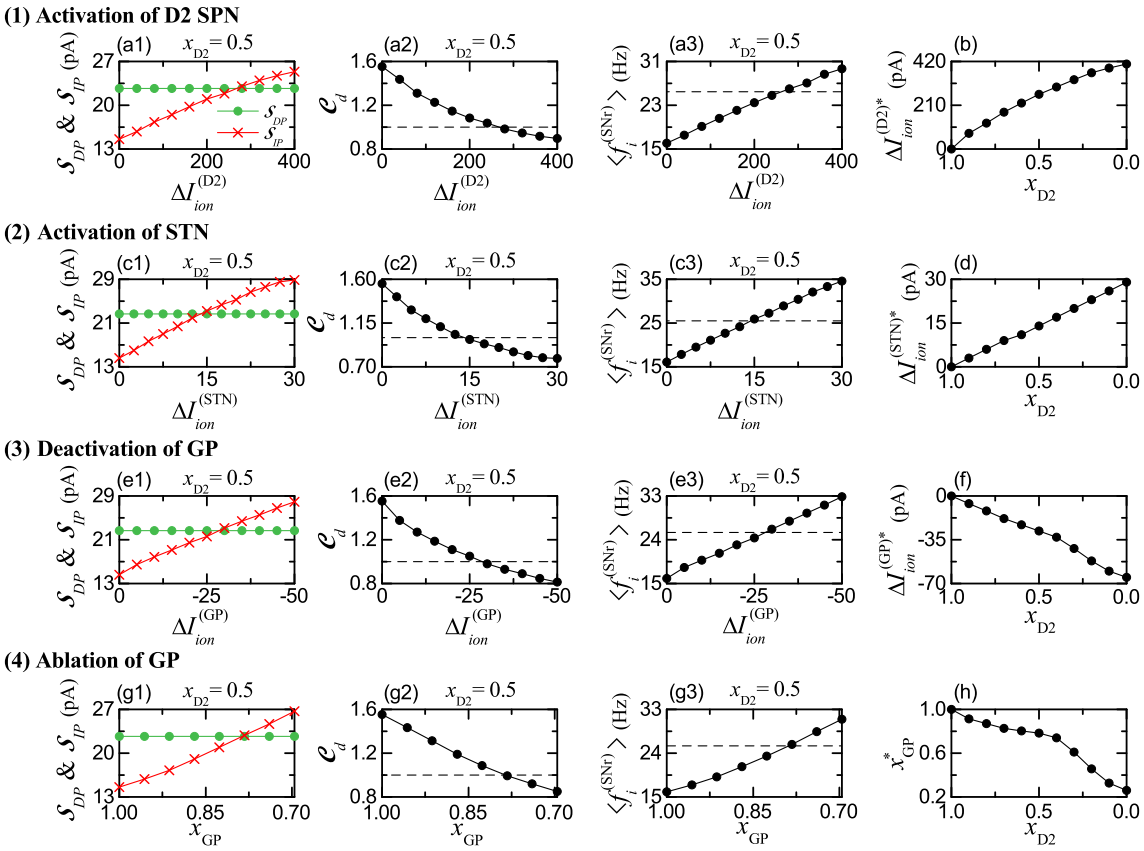

Fig. 4 Treatment of tonic pathological state by strengthening IP for the tonic cortical input (3 Hz). Colors: parts, related to DP (green), while parts, associated with IP (red). (1) Activation of D2 SPN: Plots of (a1) $\mathcal{S}_{DP}$ (green circles) and $\mathcal{S}_{IP}$ (red crosses), (a2) $\mathcal{C}_d$, and (a3) $\langle f_i^{(SNr)} \rangle$ versus $\Delta I_{ion}^{(D2)}$ for $x_{D2} = 0.5$. (b) Plot of threshold $\Delta I_{ion}^{(D2)*}$ versus x_{D2}. (2) Activation of STN: Plots of (c1) $\mathcal{S}_{DP}$ and $\mathcal{S}_{IP}$, (c2) $\mathcal{C}_d$, and (c3) $\langle f_i^{(SNr)} \rangle$ versus $\Delta I_{ion}^{(STN)}$ for $x_{D2} = 0.5$. (d) Plot of threshold $\Delta I_{ion}^{(D2)*}$ versus x_{D2}. (3) Deactivation of GP: Plots of (e1) $\mathcal{S}_{DP}$ and $\mathcal{S}_{IP}$, (e2) $\mathcal{C}_d$, and (e3) $\langle f_i^{(SNr)} \rangle$ versus $\Delta I_{ion}^{(GP)}$ for $x_{D2} = 0.5$. (f) Plot of threshold $\Delta I_{ion}^{(GP)*}$ versus x_{D2}. (4) Ablation of GP: Plots of (g1) $\mathcal{S}_{DP}$ and $\mathcal{S}_{IP}$, (g2) $\mathcal{C}_d$, and (g3) $\langle f_i^{(SNr)} \rangle$ versus x_{GP} for $x_{D2} = 0.5$. (h) Plot of threshold x_{GP}^* versus x_{D2}. Horizontal dashed lines in (a2), (c2), (e2), and (g2) represent $\mathcal{C}_d^*$ (= 1.0) for the default healthy tonic state when $x_{D2} = 1$. Horizontal dashed lines in (a3), (c3), (e3), and (g3) represent $\langle f_i^{(SNr)} \rangle$ (=25.5 Hz) for the default healthy tonic state when $x_{D2} = 1$

with $\mathcal{C}_d = 1.53$ may have $\mathcal{C}_d$ (= 1.0) via activation of D2 SPNs for the threshold, $\Delta I_{ion}^{(D2)*}$ (= 262 pA); DP and IP becomes balanced, as in the case of tonic healthy state. In this way, balance between DP and IP is recovered for $\Delta I_{ion}^{(D1)*}$ = 262 pA. Figure 4b shows the plot of $\Delta I_{ion}^{(D2)*}$ versus x_{D2}. As x_{D2} is decreased from 1, the threshold $\Delta I_{ion}^{(D2)*}$ is increased; with decreasing x_{D2}, more $\Delta I_{ion}^{(D2)*}$ is necessary for recovery of balance between DP and IP.

We also strengthen the IP via activation of the target (under-active) STN neurons, which is shown in Fig. 4c1–c3 for $x_{D2} = 0.5$. All the behaviors are qualitatively the same as those in the case of activation of D2 SPNs. With increasing $\Delta I_{ion}^{(STN)}$ from 0, $\mathcal{S}_{IP}$ (strength of IP) increases, leading to decrease in the competition degree $\mathcal{C}_d$, and the population-averaged MFR of the output SNr neurons, $\langle f_i^{(SNr)} \rangle$, also increases. But, the threshold $\Delta I_{ion}^{(STN)*}$ (= 14 pA), where balance between DP and IP is recovered (i.e., $\mathcal{C}_d$ = 1 and $\langle f_i^{(SNr)} \rangle$ = 25.5 Hz, as in the case of tonic healthy state), is smaller than that (262 pA) in the case of activation of D2 SPNs. The mono-synaptic effect of STN neurons on the output SNr neurons is more direct than the bi- or tri-synaptic effect of D2 SPNs, which could result in the smaller threshold $\Delta I_{ion}^{(STN)*}$ in the case of STN neurons. Figure 4d shows the plot of $\Delta I_{ion}^{(STN)*}$ versus x_{D2}. With decreasing x_{D2} from 1, the threshold $\Delta I_{ion}^{(STN)*}$ increases, as shown in Fig. 4d; As x_{D2} is decreased, more $\Delta I_{ion}^{(STN)*}$ is necessary for recovery of balance between DP and IP.

Unlike the cases of activation of (under-active) D2 SPNs and STN neurons, IP may be strengthened via deactivation of (over-active) GP neurons; in the case of deactivation, $\Delta I_{ion}^{(GP)}$ is negative, in contrast to the case of activation with

$\Delta I_{ion}^{(X)} > 0$ [X = D2 (SPN) and STN]. Figure 4e1–e3 and f show the case of deactivation of GP neurons. As the magnitude of $\Delta I_{ion}^{(GP)}$ is increased (i.e., more negative), strength of IP, $\mathcal{S}_{IP}$ (red), is found to increase from 15.1, while $\mathcal{S}_{DP}$ (green) remains constant (= 23.1). Thus, when passing a threshold $\Delta I_{ion}^{(GP)*} = -28$ pA, balance between DP and IP becomes recovered (i.e., the competition degree $\mathcal{C}_d$ becomes 1 and the population-averaged MFR of output SNr neurons $\langle f_i^{(SNr)} \rangle$ becomes 25.5 Hz) [see Fig. 4e2–e3]. As shown in Fig. 4f, with decreasing x_{D2} from 1, the threshold $\Delta I_{ion}^{(GP)*}$ is decreased (i.e., its magnitude increases); as x_{D2} is decreased from 1, more negative $\Delta I_{ion}^{(GP)*}$ is required for recovery of balance between DP and IP.

Instead of the above deactivation of GP neurons via optogenetics, we also consider ablation of (over-active) GP neurons in the pathological state for $x_{D2} = 0.5$ to reduce the over-activity of GP neurons. In the case of ablation, the number of GP neurons, N_{GP}, is reduced to $N_{GP}^{(n)}$ x_{GP} ($1 > x_{GP} > 0$), where $N_{GP}^{(n)}$ (= 46) is the normal number of GP neurons and x_{GP} is the fraction of number of GP neurons. As shown in Fig. 4g1–g3 and h, the effect of decreasing x_{GP} via ablation is similar to that of deactivation of GP neurons via optogenetics. As x_{GP} is decreased from 1, strength of IP, $\mathcal{S}_{IP}$ (red), is found to increase from 15.1 (i.e., IP becomes strengthened) [see Fig. 4g1]. When passing a threshold, x_{GP}^* ($\simeq 0.78$), balance between DP and IP becomes recovered (i.e., $\mathcal{C}_d$ = 1.0 and $\langle f_i^{(SNr)} \rangle$ = 25.5 Hz), as shown in Fig. 4g2–g3. Figure 4h shows the plot of x_{GP}^* versus x_{D2}. With decreasing x_{D2} from 1, x_{GP}^* decreases; more ablation (i.e., smaller x_{GP}) is necessary for balance between DP and IP.

Next, we consider phasic pathological states with enhanced competition degree $\mathcal{C}_d$ [larger than that (2.82) for the phasic healthy state (with harmony between DP and IP)], occurring due to degenerative loss of D2 SPNs, in the case of phasic cortical input (10 Hz) (see Fig. 3). As an example, we consider the pathological case of $x_{D2} = 0.5$ with $\mathcal{C}_d = 7.19$. In this phasic pathological case, IP is under-active in comparison to the case of phasic healthy state. For the phasic healthy state with $\mathcal{C}_d^*$ = 2.82 (i.e., harmony between DP and IP), the population-averaged MFR of output STr neurons, $\langle f_i^{(SNr)*} \rangle$, is much reduced to 5.5 Hz, leading to normal movement, in contrast to the case of tonic healthy state with $\mathcal{C}_d \simeq 1.0$ and $\langle f_i^{(SNr)} \rangle$ = 25.5 Hz without movement. As in the above tonic pathological state, firing activity of D2 SPNs is under-active, resulting in over-activity of GP neurons, which then leads to under-activity of the STN neurons. Hence, for recovery of harmony between DP and IP, we strengthen the IP through activation of D2 SPNs and STN neurons and deactivation of GP neurons by employing optogenetic technique and via ablation of GP neurons.

Figure 5 shows treatment of phasic pathological state for $x_{D2} = 0.5$ with $\mathcal{C}_d = 7.19$; (1) activation of D2 SPNs, (2) activation of STN neurons, (3) deactivation of GP neurons, and (4) ablation of GP neurons. The overall results of these treatments are qualitatively the same as those in the above case of tonic pathological state in Fig. 4. Only the corresponding thresholds are quantitatively different; (1) $\Delta I_{ion}^{(D2)*}$ = 1,636 pA, (2) $\Delta I_{ion}^{(STN)*}$ = 405 pA, (3) $\Delta I_{ion}^{(GP)*} = -540$ pA, and (4) x_{GP}^* ($\simeq 0.52$). When passing a threshold for each treatment, harmony between DP and IP becomes recovered (i.e., $\mathcal{C}_d$ = 2.82 and $\langle f_i^{(SNr)} \rangle$ = 5.5 Hz), resulting in normal movement. Finally, we note that, with decreasing x_{D2}, the thresholds, $\Delta I_{ion}^{(D2)*}$ and $\Delta I_{ion}^{(STN)*}$, for activations of D2 SPNs and STN neurons are increased (i.e., more positive), and the threshold, $\Delta I_{ion}^{(GP)*}$ for deactivation of GP neurons becomes more negative, as shown in Fig. 5b, d, and f. Thus, as x_{D2} is decreased, more light stimulation for activation and deactivation is necessary for recovery of harmony between DP and IP. Also, in the case of ablation of GP neurons, with decreasing x_{D2}, more ablation is required to get harmony between DP and IP.

Effect of loss of healthy synapses on the HD

In the HD, loss of healthy synapses occurs not only in the striatum, but also in other regions of the BG, including STN, GP, and SNr (Reiner et al. 1988; Klapstein et al. 2001; Cepeda et al. 2007; Milnerwood and Raymond 2010; Milnerwood et al. 2010; Plotkin, and Surmeier 2015). Such loss of synapses in the BG neurons is an important feature of HD, and it is thought to contribute to the motor and cognitive symptoms of the disease. Here, we study effect of loss of healthy synapses of all the BG neurons on HD.

As examples, we consider pathological states for x_{D2} = 0.5 in both cases of tonic (3 Hz) and phasic (10 Hz) cortical inputs. Loss of synapses in the BG neurons is modeled in terms of decreased synaptic connection probability, $p_c = p_c^{(n)}\, x_c$; $p_c^{(n)}$ is the normal synaptic connection probability (depending on the type of BG neurons and given in Table II in (Kim and Lim 2023)) and x_c represents the fraction in p_c ($1 > x_c > 0$).

We first consider a tonic pathological state in Fig. 6a–c. As a result of loss of synapses, decreased cortical inputs into D1 SPNs leads to reduction in their firing activity $\langle f_i^{(D1)} \rangle$. Then, strength of DP, $\mathcal{S}_{DP}$, becomes decreased. As shown in Fig. 6a, $\mathcal{S}_{DP}$ (green color) is found to monotonically decrease from 23.1 with decreasing x_c from 1. Also, due to reduced cortical synaptic inputs into D2 SPNs, firing activity of D2 SPNs, $\langle f_i^{(D2)} \rangle$, becomes decreased, leading to

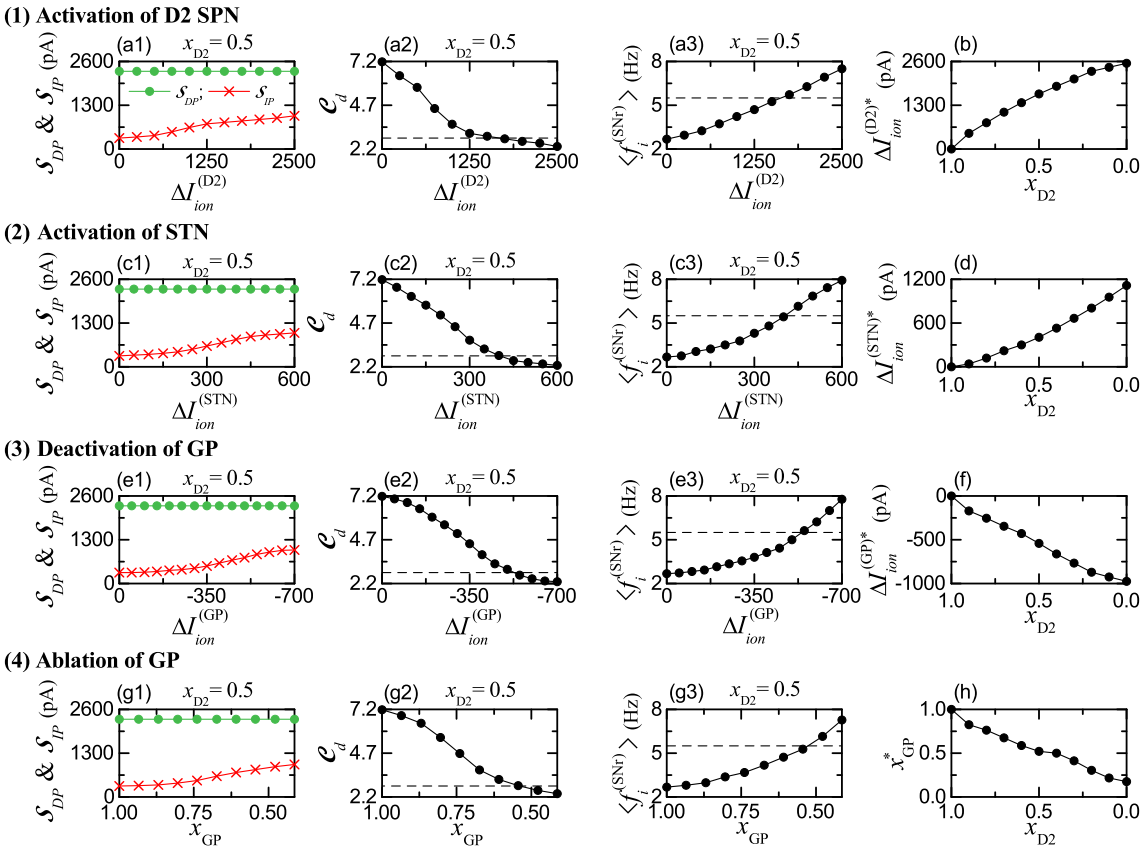

Fig. 5 Treatment of phasic pathological state by strengthening IP for the phasic cortical input (10 Hz). Colors: parts, related to DP (green), while parts, associated with IP (red). (1) Activation of D2 SPN: Plots of **a1** $\mathcal{S}_{DP}$ and $\mathcal{S}_{IP}$, **a2** $\mathcal{C}_d$, and **a3** $\langle f_i^{(SNr)} \rangle$ versus $\Delta I_{ion}^{(D2)}$ for $x_{D2} = 0.5$. **b** Plot of threshold $\Delta I_{ion}^{(D2)*}$ versus x_{D2}. (2) Activation of STN: Plots of **c1** $\mathcal{S}_{DP}$ and $\mathcal{S}_{IP}$, **c2** $\mathcal{C}_d$, and **c3** $\langle f_i^{(SNr)} \rangle$ versus $\Delta I_{ion}^{(STN)}$ for $x_{D2} = 0.5$. **d** Plot of threshold $\Delta I_{ion}^{(STN)*}$ versus x_{D2}. (3) Deactivation of GP: Plots of **e1** $\mathcal{S}_{DP}$ and $\mathcal{S}_{IP}$, **e2** $\mathcal{C}_d$, and **e3** $\langle f_i^{(SNr)} \rangle$ versus $\Delta I_{ion}^{(GP)}$ for $x_{D2} = 0.5$. **f** Plot of threshold $\Delta I_{ion}^{(GP)*}$ versus x_{D2}. (4) Ablation of GP: Plots of **g1** $\mathcal{S}_{DP}$ and $\mathcal{S}_{IP}$, **g2** $\mathcal{C}_d$, and **g3** $\langle f_i^{(SNr)} \rangle$ versus x_{GP} for $x_{D2} = 0.5$. **h** Plot of threshold x_{GP}^* versus x_{D2}. Horizontal dashed lines in (a2), (c2), (e2), and (g2) represent $\mathcal{C}_d^*$ (= 2.82) for the healthy phasic state when $x_{D2} = 1$. Horizontal dashed lines in (a3), (c3), (e3), and (g3) represent $\langle f_i^{(SNr)} \rangle$ (= 5.5 Hz) for the healthy phasic state when $x_{D2} = 1$

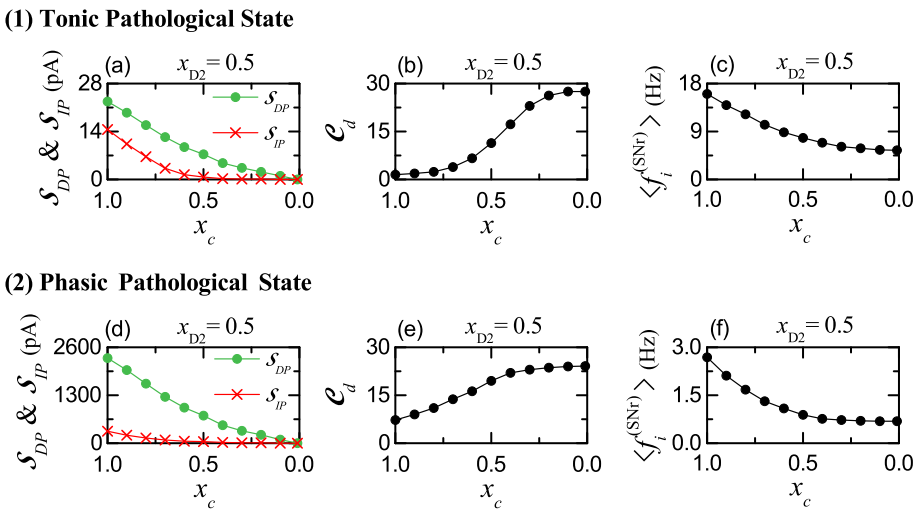

Fig. 6 Effect of loss of healthy synapses in all the BG neurons on the HD for $x_{D2} = 0.5$. Colors: parts, related to DP (green), while parts, associated with IP (red). (1) Tonic pathological state: Plots of **a** $\mathcal{S}_{DP}$ and $\mathcal{S}_{IP}$, **b** $\mathcal{C}_d$, and **c** $\langle f_i^{(SNr)} \rangle$ versus x_c. (2) Phasic pathological state: Plots of **d** $\mathcal{S}_{DP}$ and $\mathcal{S}_{IP}$, **e** $\mathcal{C}_d$, and **f** $\langle f_i^{(SNr)} \rangle$ versus x_c

increased firing activity of GP neurons ($\langle f_i^{(\mathrm{GP})} \rangle$), which then results in decrease in the firing activity of STN neurons ($\langle f_i^{(\mathrm{STN})} \rangle$). Consequently, strength of IP, $\mathcal{S}_{IP}$, becomes decreased. In this case of IP, with decreasing x_c from 1, $\mathcal{S}_{IP}$ (red color) is found to more rapidly decrease from 15.1 than the case of DP. Then, the competition $\mathcal{C}_d$ between DP and IP increases rapidly from 1.53 with decreasing x_c from 1 [see Fig. 6b]. Thus, as x_c is decreased from 1, population-averaged MFR of the output SNr neurons ($\langle f_i^{(\mathrm{SNr})} \rangle$) decreases from 16.1 Hz. In this way, with decreasing x_c, the degree of disharmony between DP and IP becomes increased, resulting in more severe involuntary jerky movement in the tonic pathological case.

Next, we consider a phasic pathological state in Fig. 6d–f. With decreasing x_c, tendency in the phasic pathological case is qualitatively the same as that in the above tonic pathological case. Based on the same reasoning given in the tonic pathological case, as x_c is decreased from 1, strength of IP ($\mathcal{S}_{IP}$; red color) is found to decreases much more rapidly than strength of DP ($\mathcal{S}_{DP}$; green color), as shown in Fig. 5d. Then, the competition degree $\mathcal{C}_d$ increases from 7.19 with decreasing x_c from 1 [see Fig. 5e]. Consequently, firing activity of the output SNr neurons ($\langle f_i^{(\mathrm{SNr})} \rangle$) decreases from 2.7 Hz with x_c, as shown in Fig. 5f. In this way, as x_c is decreased from 1, the broken-up degree of harmony between DP and IP becomes increased, leading to more severe abnormal hyperkinetic movement disorder in the phasic pathological case.

Overall, in both tonic and phasic pathological cases, as a result of loss of healthy synapses in the BG neurons, symptoms of the HD become more severe with decreasing x_c, because the disharmony degree between DP and IP becomes increased.

Summary and discussion

The BG exhibit a variety of functions for motor, cognition, and emotion. Dysfunction in the BG is associated with movement disorder (e.g., HD and PD) and cognitive and psychiatric disorders. There are two competing pathways in the BG, DP (facilitating movement) and IP (suppressing movement) (Albin et al. 1989; Alexander and Crutcher 1990; DeLong 1990; Kravitz et al. 2010). In our recent work (Kim and Lim 2023), as a first time, we made quantitative analysis of competitive harmony between DP and IP in the default tonic state and the phasic healthy and pathological states by introducing their competition degree, $\mathcal{C}_d$, between DP and IP, given by the ratio of strength of DP ($\mathcal{S}_{DP}$) to strength of IP ($\mathcal{S}_{IP}$) (i.e., $\mathcal{C}_d = \mathcal{S}_{DP}/\mathcal{S}_{IP}$).

In our prior work (Kim and Lim 2023), we studied PD which was found to occur for lower DA level. In the case of PD with reduced competition degree, IP is over-active, while DP is under-active, leading to abnormal hypokinetic movement.

In this paper, we are concerned in the HD which is a genetic neurodegenerative disease. We considered the early stage of HD where the DA level is normal. As a result of mutant HTT gene, toxic HTT protein aggregates appear, causing the characteristic neurodegeneration seen in HD. We considered degenerative loss of D2 SPNs in the case of normal DA level. By decreasing x_{D2} (i.e. fraction of number of D2 SPNs) from 1, we quantitatively analyzed break-up of harmony between DP and IP. IP was found to be under-active (i.e., weakened), in contrast to the case of PD with over-active IP. Thus, the competition degree $\mathcal{C}_d$ becomes increased than normal one. Consequently, abnormal hyperkinetic movement such as chorea occurs, in contrast to the case of PD with hypokinetic disorder.

Unfortunately, at present there is no cure for HD. The available treatments for HD primarily aim to control and alleviate its symptoms, resulting from weakened IP: medication treatment (Hayden et al. 2009; Bashir and Jakovic 2018; Luis-Ravelo et al. 2018; Bachoud-Lévi et al. 2019), reducing symptoms, deep brain stimulation in research and clinical trials (Nagel et al. 2015; Sharma and Deogaonkar 2015; Wojtecki et al. 2016; Yin et al. 2023), and experimental surgery (Demeestere and Vandenberghe 2011). Here, we studied treatment of HD via recovery of harmony between DP and IP by activating D2 SPNs and STN neurons and deactivating GP neurons, based on optogenetics (Kravitz et al. 2010; Tecuapetla et al. 2014). Through the treatment process, the IP becomes strengthened, and thus harmony between DP and IP may be regained. The results for the 3 optogenetic targets (D2 SPN, STN, GP) are well shown in Figs. 4 and 5. We note that in the case of STN, the magnitude of threshold $\Delta I_{ion}^{(\mathrm{STN})*}$ where harmony between DP and IP is recovered is the lowest, because the mono-synaptic effect of STN neurons on the output nucleus SNr is more direct than the bi- and tri-synaptic effect of D2 SPNs and GP cells. Hence, the STN could be the most effective target for optogenetic treatment. We also studied effects of loss of healthy synapses of the BG cells on the HD. As healthy synapses are lost in the BG, strength of the IP is found to decrease more rapidly than the case of the DP, resulting in increase in disharmony between DP and IP increases. Consequently, symptoms of the HD become worse. In this case of synapse loss, optogenetics and GP ablation are also expected to be effectively used for treatment. But, the threshold values of treatment could increase in comparison to the case without loss of healthy synapses, because the symptoms of HD are worse in the case of synapse loss.

We also make overall summary of our basic underlying approach for study of the BG function. The SNr is the output nucleus of the BG, providing inhibitory projection to the thalamus. Firing activity of the SNr is well characterized in terms of their population-averaged MFR $\langle f_i^{(\mathrm{SNr})} \rangle$. When $\langle f_i^{(\mathrm{SNr})} \rangle$ is high (low), the BG gate to the thalamus becomes locked (opened), leading to inhibition (disinhibition) of the thalamus. In this way, the population-averaged MFR of the SNr, $\langle f_i^{(\mathrm{SNr})} \rangle$, is a good indicator for the functional activity of the BG. So, in Figs. 2, 3, 4 and 5, we examined variation in $\langle f_i^{(\mathrm{SNr})} \rangle$ with respect to change in x_{D2} (fraction of the number of D2 SPNs) and in variation in intrinsic ionic current $\Delta I_{ion}^{(X)}$ due to optogenetics.

We note that firing activity (i.e. MFR) of the SNr is determined via competition between the DP synaptic current and the IP synaptic current into the SNr. Their competition may be well characterized in terms of our recently-introduced competition degree C_d, given by the ratio of the strength of DP to the strength of IP (Kim and Lim 2023). Thus, C_d plays a good role of indicator for the synaptic inputs into the SNr, in contrast to the output indicator, $\langle f_i^{(\mathrm{SNr})} \rangle$. Hence, relationship between C_d and $\langle f_i^{(\mathrm{SNr})} \rangle$ may be regarded as the cause-and-effect. The larger C_d is, the lower $\langle f_i^{(\mathrm{SNr})} \rangle$. We obtained C_d and $\langle f_i^{(\mathrm{SNr})} \rangle$ in our BG SNN, well shown in Figs. 2, 3, 4 and 5. In this sense, we emphasize that C_d and $\langle f_i^{(\mathrm{SNr})} \rangle$ are basic quantities characterizing the BG functional activity. In future, it would be interesting to try to get C_d and $\langle f_i^{(\mathrm{SNr})} \rangle$ in the mean field model for comparison (Tesler et al. 2022). For such comparison, mean-field approach must be developed to obtain not only the population-averaged output $\langle f_i^{(\mathrm{SNr})} \rangle$ of the SNr, but also the population-averaged DP and IP synaptic input currents into the SNr.

Finally, we discuss limitations of our present work and future works. In the present work, we considered early stage of HD where degenerative loss of D2 SPNs occurs in the nearly normal DA level. But, in the late stage of HD, degenerative loss of D1 SPN also occurs along with decrease in DA level, leading to hypokinetic disorder (e.g., rigidity and bradykinesia) due to weakened DP, as in the case of PD (Berardelli et al. 1999). Moreover, in addition to deaths of D1/D2 SPNs, degeneration of cortical pyramidal cells occurs (Cudkowicz and Kowall 1990; Hedreen et al. 1991). Hence, as a future work, it would be interesting to investigate consequences of degeneration of D1 SPNs and cortical pyramidal cells, in addition to degenerative loss of D2 SPNs.

Next, we would like to consider more realistic striatal circuit in the BG. In our present striatal circuit, we considered only the D1/D2 SPNs (95 % major population). But, the minor population of fast interneurons (FSIs) in the striatum are known to exert strong effects on firing activities of the D1/D2 SPNs (Koós and Tepper 1999; Humphries et al. 2009b). Hence, in future, it would be worth while to contain the FSIs in our BG SNN. In addition, lateral connections between D1 SPNs and D2 SPNs also exists in the striatum (Mark et al. 2010; Tomkins et al. 2014). Thus, it would be worth while to contain lateral connections between D1 SPNs and D2 SPNs in our BG SNN and investigate the HD state and treatment. In our present BG SNN, cortical inputs were modelled by Poisson spike trains. Such SNN could be extended to the cortico-BG-thalamo-cortical (CBGTC) loop by including the cortical and the thalamic neurons for more complete computational work (Narayanan 2003; Navarro-López et al. 2021).

We also make discussion on application of the optogenetics to human patients for treatment of a pathological state (Gittis and Yttri 2018; Shen et al. 2020). In the case of HD, harmony between DP and IP is broken up due to under-active IP. As shown in Sec. 2.2, harmony between DP and IP could be recovered by strengthening IP. To this end, optogenetic techniques may be employed. Activation of D2 SPNs and STN neurons via optogenetics results in strengthening IP. We hope that, in near future, safe clinical applications of optogenetics to human patients with HD could be successfully available via collaboration of researchers and clinicians. Then, it would take a substantial step forward for treatment of HD.

We note that the optogenetic treatment could have benefits in comparison to the traditional deep-brain-stimulation (DBS) treatment. The DBS has the following disadvantages (Gittis and Yttri 2018; Shen et al. 2020); (a) it is difficult to accurately determine the target cells, leading to cause many side effects and (b) a process with many trial and errors is necessary to each patient for optimal control. On the other hand, the target cells can be accurately located by optogenetic stimulation. Hence, side effects and trial-and-error process may be decreased in spite of limitations for application to the human patients (Gittis and Yttri 2018).

Supplementary Information The online version contains supplementary material available at https://doi.org/10.1007/s11571-024-10125-w.

Acknowledgements This research was supported by the Basic Science Research Program through the National Research Foundation of Korea (NRF) funded by the Ministry of Education (Grant No. 20162007688).

Conflict of interest The authors declare that they have no Conflict of interest.

References

Albin RL, Reiner A, Anderson KD, Dure LS, Handelin B, Balfour R, Whetsell WO Jr, Penney JB, Young AB (1992) Preferential loss of striato-external pallidal projection neurons in presymptomatic Huntington's disease. Ann Neurol 31:425–430

Albin RL, Young AB, Penne JB (1989) The functional anatomy of basal ganglia disorders. Trends Neurosci 12:366–375

Alexander GE, Crutcher MD (1990) Functional architecture of basal ganglia circuits: neural substrates of parallel processing. Trends Neurosci 13:266–272

Ammari R, Bioulac B, Garcia L, Hammond C (2011) The subthalamic nucleus becomes a generator of bursts in the dopamine-depleted state its high frequency stimulation dramatically weakens transmission to the globus pallidus. Front Syst Neurosci 5:43

Andres DS, Darbin O (2018) Complex dynamics in the basal ganglia: health and disease beyond the motor system. J Neuropsychiatry Clin Neurosci 30:101–114

Armstrong MJ, Okun MS (2020) Diagnosis and treatment of Parkinson disease: a review. JAMA 323:548–560

Bachoud-Lévi AC, Ferreira J, Massart R, Youssov K, Rosser A, Busse M, Craufurd D, Reilmann R, Michele GD, Rae D, Squitieri F, Seppi K, Perrine C, Scherer-Gagou C, Audrey O, Verny C, Burgunder JM (2019) International guidelines for the treatment of Huntington's disease. Front Neurol 10:710

Bar-Gad I, Morris G, Bergman H (2003) Information processing, dimensionality reduction and reinforcement learning in the basal ganglia. Prog Neurobiol 71:439–473

Bashir H, Jakovic J (2018) Treatment options for chorea. Expert Rev Neurother 18:51–63

Bates GP (2005) History of genetic disease: the molecular genetics of Huntington disease - A history. Nat Rev Genet 6:766–773

Bates GP, Dorsey R, Gusella JF, Hayden MR, Kay C, Leavitt BR, Nance M, Ross CA, Scahill RI, Wetzel R, Wild EJ, Tabrizi SJ (2015) Huntington disease. Nat Rev Dis Primers 1:15005

Baufreton J, Atherton JF, Surmeier DJ, Bevan MD (2005) Enhancement of excitatory synaptic integration by GABAergic inhibition in the subthalamic nucleus. J Neurosci 25:8505–8517

Bauswein E, Fromm C, Preuss A (1989) Corticostriatal cells in comparison with pyramidal tract neurons: contrasting properties in the behaving monkey. Brain Res 493:198–203

Bear MF, Connors BM, Paradiso MA (2007) Neuroscience: Exploring the Brain. Lippincott Williams & Wikins, Philadelphia

Belforte JE, Zsiros V, Sklar ER, Yu Jiang ZG, Li Y, Quinlan EM, Nakazawa K (2010) Postnatal NMDA receptor ablation in corticolimbic interneurons confers schizophrenia-like phenotypes. Nat Neurosci 13:76–83

Berardelli A, Noth J, Thompson PD, Bollen EL, Curra A, Deuschl G, van Dijk JG, Topper R, Schwarz M, Roos RA (1999) Pathophysiology of chorea and bradykinesia in Huntington's disease. Mov Disord 14:398–403

Bevan MD, Wilson CJ (1999) Mechanisms underlying spontaneous oscillation and rhtymic firing in rat subthalamic neurons. J Neurosci 19:7617–7628

Bevan MD, Wilson CJ, Bolam JP, Magill PJ (2000) Equilibrium potential of GABA-A current and implications for rebound burst firing in rat subthalamic neurons in vitro. J Neurophysiol 83:3169–3172

Bevan MD, Magill PJ, Hallworth NE, Bolam JP, Wilson CJ (2002) Regulation of the timing and pattern of action potential generation in rat subthalamic neurons in vitro by GABA-A IPSPs. J Neurophysiol 87:1348–1362

Bolam JP, Bergman H, Graybiel AM, Kimura M, Plenz D, Seung HS, Surmeier DJ, Wickens JR (2006) Microcircuits in the striatum. In: Grillner S, Graybiel AM (eds) Microcircuits: The Interface Between Neurons and Global Brain Function. MIT Press, Cambridge, pp 165–190

Brunel N, Hakim V (2008) Sparsely synchronized neuronal oscillations. Chaos 18:015113

Brunel N, Wang XJ (2003) What determines the frequency of fast network oscillations with irregular neural discharges? I. Synaptic dynamics and excitation-inhibition balance. J Neurophysiol 90:415–430

Bugaysen J, Bronfeld M, Tischler H, Bar-Gad I, Korngreen A (2010) Electrophysiological characteristics of globus pallidus neurons. PLOS One 5:e12001

Cakir Y (2019) The synchronization behavior of basal ganglia. J Cogn Syst 4:38–45

Celikok U, Sengör NS (2016) Realizing medium spiny neurons with a simple neuron model. Poster session presentation at the meeting of the international conference on artificial neural networks, Barcelona, Spain

Celikok U, Navarro-López EM, Sengör NS (2016) A computational model describing the interplay of basal ganglia and subcortical background oscillations during working memory processes. arXiv https://doi.org/10.48550/arXiv.1601.07740

Cepeda C, Wu N, André VM, Cummings DM, Levine MS (2007) The corticostriatal pathway in Huntington's disease. Prog Neurobiol 81:253–271

Connelly WM, Schulz JM, Lees G, Reynolds JN (2010) Differential short-term plasticity at convergent inhibitory synapses to the substantia nigra pars reticulata. J Neurosci 30:14854–14861

Crossman AR (1987) Primate models of dyskinesia: the experimental approach to the study of basal gangliarelated involuntary movement disorders. Neurosci 21:1–40

Crossman AR, Mitchell IJ, Sambrook MA, Jackson A (1988) Chorea and myoclonus in the monkey induced by gamma-aminobutyric acid antagonism in the lentiform complex. The site of drug action and a hypothesis for the neural mechanisms of chorea. Brain 111:1211–1233

Cudkowicz M, Kowall NW (1990) Degeneration of pyramidal projection neurons in Huntington's disease cortex. Ann Neurol 27:200–204

Dayan P, Abbott LF (2001) Theoretical Neuroscience. MIT Press, Cambridge

DeLong MR (1990) Primate models of movement disorders of basal ganglia origin. Trends Neurosci 13:281–285

Demeestere J, Vandenberghe W (2011) Experimental surgical therapies for Huntington's disease. CNS Nuerosci Ther 17:705–713

Fountas Z (2016) Action Selection in The Rhythmic Brain: The Role of The Basal Ganglia and Tremor. PhD thesis, Imperial College London

Fountas Z, Shanahan M (2014a) GPU-based fast parameter optimization for phenomenological spiking neural models. international joint conference on neural networks (IJCNN) pp 1–8

Fountas Z, Shanahan M (2014b) Phase offset between slow oscillatory cortical inputs influences competition in a model of basal ganglia. International Joint Conference on Neural Networks (IJCNN) 2407-2414

Fountas Z, Shanahan M (2017a) The role of cortical oscillations in a spiking neural network model of the basal ganglia. PLOS ONE 12:e0189109

Fountas Z, Shanahan M (2017b) Assessing selectivity in the basal ganglia: The 'Gearbox' hypothesis. BioRxiv. https://doi.org/10.1101/197129

Frank MJ (2005) Dynamic dopamine modulation in the basal ganglia: a neurocomputational account of cognitive deficits in medicated and non-medicated Parkinsonism. J Cogn Neurosci 17:51–72

Frank MJ, Loughry B, O'Reilly RC (2001) Interactions between frontal cortex and basal ganglia in working memory: a computational model. Cogn Affect Behav Neurosci 1:137–160

Frank MJ, Seeberger LC, O'Reilly RC (2004) By carrot or by stick: cognitive reinforcement learning in Parkinsonism. Science 306:1940–1943

Fujimoto K, Kita H (1993) Response characteristics of subthalamic neurons to the stimulation of the sensorimotor cortex in the rat. Brain Res 609:185–192

Geisler C, Brunel N, Wang XJ (2005) Contributions of intrinsic membrane dynamics to fast network oscillations with irregular neuronal discharges. J Neurophysiol 94:4344–4361

Gertler TS, Chan CS, Surmeier DJ (2008) Dichotomous anatomical properties of adult striatal medium spiny neurons. J Neurosci 28:10814–10824

Gittis AH, Yttri EA (2018) Translating insights from optogenetics into therapies for Parkinson's disease. Curr Opin Biomed Eng 8:14–19

Góngora-Alfaro JL, Hernández-López S, Flores-Hernández J, Galarraga E (1997) Firing frequency modulation of substantia nigra reticulata neurons by 5-hydroxytryptamine. Neurosci Res 29:225–231

González-Redondo Á, Naveros F, Ros E, Garrido JA (2020) A basal ganglia computational model to explain the paradoxical sensorial improvement in the rresence of Huntington's disease. Int J Neural Syst 30:2050057

Goodliffe JW, Song H, Rubakovic A, Chang W, Medalla M, Weaver CM, Lübke JI (2018) Differential changes to D1 and D2 medium spiny neurons in the 12-month-old Q175$^{+/-}$ mouse model of Huntington's Disease. PLOS ONE 13:e0200626

Götz T, Kraushaar U, Geiger J, Lübke J, Berger T, Jonas P (1997) Functional properties of AMPA and NMDA receptors expressed in identified types of basal ganglia neurons. J Neurosci 17:204–215

Guridi J, González-Redondo R, Obeso JA (2012) Clinical features, pathophysiology, and treatment of levodopa-induced dyskinesias in Parkinson's disease. Parkinsons Dis 2012:943159

Gurney K, Prescott TJ, Redgrave P (2001a) A computational model of action selection in the basal ganglia. I A new functional anatomy. Biol Cybern 84:401–410

Gurney K, Prescott TJ, Redgrave P (2001b) A computational model of action selection in the basal ganglia. II. Analysis and simulation of behavior. Biol Cybern 84:411–423

Gusella JF, Wexler NS, Conneally PM, Naylor SL, Anderson MA, Tanzi RE, Watkins PC, Ottina K, Wallace MR, Sakaguchi AY, Young AB, Shoulson I, Bonilla E, Martin JB (1983) A polymorphic DNA marker genetically linked to Huntington's disease. Nature 306:234–238

Hallworth NE, Wilson CJ, Bevan MD (2003) Apamin-sensitive small conductance calcium-activated potassium channels, through their selective coupling to voltage-gated calcium channels, are critical determinants of the precision, pace, and pattern of action potential generation in rat subthalamic nucleus neurons in vitro. J Neurosci 23:7525–7542

Han I, You YM, Kordower JH, Brady ST, Morfini GA (2010) Differential vulnerability of neurons in Huntington's disease: the role of cell type-specific features. J Neurochem 113:1073–1091

Hayden MR, Leavitt BR, Yasothan U, Kirkpatrick P (2009) Tetrabenazine. Nat Rev Drug Discov 8:17–18

Hedreen JC, Peyser CE, Folstein SE, Ross CA (1991) Neuronal loss in layers V and VI of cerebral cortex in Huntington's disease. Neurosci Lett 133:257–261

Humphries MD (2014) Basal ganglia: Mechanisms for action selection. In: Encyclopedia of Computation Neuroscience. Springer, New York

Humphries MD, Gurney K (2021) Making decisions in the dark basement of the brain: a look back at the GPR model of action selection and the basal ganglia. Biol Cybern 115:323–329

Humphries MD, Stewart RD, Gurney KN (2006) A physiologically plausible model of action selection and oscillatory activity in the basal ganglia. J Neurosci 26:12921–12942

Humphries MD, Lepora N, Wood R, Gurney K (2009a) Capturing dopaminergic modulation and bimodal membrane behaviour of striatal medium spiny neurons in accurate, reduced models. Front Comput Neurosci 3:26

Humphries MD, Wood R, Gurney K (2009b) Dopamine-modulated dynamic cell assemblies generated by the GABAergic striatal microcircuit. Neural Netw 22:1174–1188

Humphries MD, Obeso JA, Dreyer JA (2018) Insights into Parkinson's disease from computational model of the basal ganglia. J Neurol Neurosurg Psychiatry 89:1181–1188

Izhikevich EM (2003) Simple model of spiking neurons. IEEE Trans Neural Netw 14:1569–1572

Izhikevich EM (2004) Which model to use for cortical spiking neurons? IEEE Trans Neural Netw 15:1063–1070

Izhikevich EM (2007a) Solving the distal reward problem through linkage of STDP and dopamine signaling. Cereb Cortex 17:2443–2452

Izhikevich EM (2007b) Dynamical Systems in Neuroscience: The Geometry of Excitability and Bursting. MIT Press, Cambridge

Kandel ER, Schwartz JH, Jessell TM (1991) Principles of Neural Science. McGraw-Hill, New York

Kim SY, Lim W (2014) Realistic thermodynamic and statistical-mechanical measures for neural synchronization. J Neurosci Meth 226:161–170

Kim SY, Lim W (2023) Quantifying harmony between direct and indirect pathways in the basal ganglia; healthy and Parkinsonian states. bioRxiv https://doi.org/10.1101/2023.09.19.558549

Klapstein GJ, Fisher RS, Zanjani H, Cepeda C, Jokel ES, Chesselet MF, Levine MS (2001) Electrophysiological and morphological changes in striatal spiny neurons in R6/2 Huntington's disease transgenic mice. J Neurophysiol 86:2667–2677

Koós T, Tepper JM (1999) Inhibitory control of nestriatal projection neurons by GABAergic interneurons. Nature Neurosci 2:467–472

Kravitz AV, Freeze BS, Parker PRL, Kay K, Thwin MT, Deisseroth K, Kreitzer AC (2010) Regulation of Parkinsonian motor behaviours by optogenetic control of basal ganglia circuitry. Nature 466:622–626

Kumaravelu K, Brocker DT, Grill WM (2016) A biophysical model of the cortex-basal ganglia-thalamus network in the 6-OHDA lesioned rat model of Parkinson's disease. J Comput Neurosci 40:207–229

Lindahl M, Kotaleski JH (2016) Untangling basal ganglia network dynamics and function: role of dopamine depletion and inhibition investigated in a spiking network model. eNeuro 3:e0156

Lindahl M, Sarvestani IK, Ekeberg O, Kotaleski JH (2013) Signal enhancement in the output stage of the basal ganglia by synaptic short-term plasticity in the direct, indirect, and hyperdirect pathways. Front Comput Neurosci 7:76

Liu X, Zhang Q, Wang Y, Chen F (2022) Electrophysiological characterization of substantia nigra pars reticulata an anesthetized rats. J Shanghai Jiaotong Univ (Sci) 27:505–511

Luis-Ravelo D, Estévez-Silva H, Barroso-Chinea P, Afonso-Oramas D, Salas-Hernández J, Rodríguez-Núñez J, Acevedo-Arozena A, Marcellino D, González-Hernández T (2018) Pramipexole reduces soluble mutant huntingtin and protects striatal neurons through dopamine D3 receptors in a genetic model of Huntington's disease. Exp Neurol 299:137–147

Luo L (2016) Principles of Neurobiology. Garland Science, New York

MacDonald ME, Ambrose CM, Duyao MP, Myers RH, Lin C, Srinidhi L, Barnes G, Taylor SA, James M, Groot N, MacFarlane H, Jenkins B, Anderson MA, Wexler NS, Gusella JF, Bates GP, Baxendale S, Hummerich H, Kirby S, North M, Youngman S, Mott R, Zehetner G, Sedlacek Z, Poustka A, Frischauf AM, Lehrach H, Buckler AJ, Church D, Doucettestamm L, Odonovan MC, Riba-rodriguez W, Shah M, Stanton VP, Strobel SA, Draths KM, Wales JL, Dervan P, Housman DE, Altherr M, Shiang R, Thompson L, Fielder T, Wasmuth JJ (1993) A novel gene containing a trinucleotide repeat that is expanded and unstable on Huntington's disease chromosomes. Cell 72:971–983

Mailly P, Charpier S, Menetrey A, Deniau JM (2003) Three-dimensional organization of the recurrent axon collateral network of the substantia nigra pars reticulata neurons in the rat. J Neurosci 23:5247–5257

Maith O, Escudero FV, Dinkelbach HÜ, Baladron J, Horn A, Irmen F, Kühn AA, Hamker FH (2021) A computational model-based analysis of basal ganglia pathway changes in Parkinson's disease inferred from resting-state fMRI. Eur J Neurosci 53:2278–2295

Mandali A, Rengaswamy M, Chakravarthy VS, Moustafa AA (2015) A spiking basal ganglia model;synchrony, exploration and decision making. Front Neurosci 9:191

Marino BLB, de Souza LR, Sousa KPA, Ferreira JV, Padilha EC, da Silva CHTP, Taft CA, Hage-Melim LIS (2020) Parkinson's disease: a review from pathophysiology to treatment. Mini Rev Med Chem 20:754–767

Mark MD, Wood R, Gurney K (2010) Reconstructing the three-dimensional GABAergic microcircuit of the striatum. PLOS Comput Biol 6:e1001011

Michmizos KP, Nikita KS (2011) Local field potential driven Izhikevich model predicts a subthalamic nucleus neuron activity. In: Engineering in medicine and biology society, EMBC, 2011 annual international conference of the IEEE, IEEE, pp. 5900–5903

Milnerwood AJ, Raymond LA (2010) Early synaptic pathophysiology in neurodegeneration: insights from Huntington's disease. Trends Neurosci 33:513–523

Milnerwood AJ, Gladding CM, Pouladi MA, Kaufman AM, Hines RM, Boyd JD, Ko RW, Vasuta OC, Graham RK, Hayden MR, Murphy TH, Raymond LA (2010) Early increase in extrasynaptic NMDA receptor signaling and expression contributes to phenotype onset in Huntington's disease mice. Neuron 65:178–190

Moyer J, Wolf JA, Finkel LH (2007) Effects of dopaminergic modulation on the integrative properties of the ventral striatal medium spiny neuron. J Neurophysiol 98:3731–3748

Mulcahy G, Atwood B, Kuznetsov A (2020) Basal ganglia role in learning rewarded actions and executing previously learned choices: healthy and diseased states. PLOS ONE 15:e0228081

Nagel SJ, Machado AG, Gale JT, Lobel DA, Pandya M (2015) Preserving cortico-striatal function: deep brain stimulation in Huntington's disease. Front Syst Neurosci 9:32

Nakanishi H, Kita H, Kitai ST (1990) Intracellular study of rat entopeduncular nucleus neurons in an in vitro slice preparation: electrical membrane properties. Brain Res 527:81–88

Narayanan S (2003) The role ofcortico-basal-thalamic loops in cognition: a computational model and preliminary results. Neurocomput 52–54:605–614

Navarro-López EM, Celikok U, Sengör NS (2016) Chapter 9 - Hybrid systems neuroscience. In: Hady AE (ed) Closed Loop Neuroscience. Elsevier, London, pp 113–129

Navarro-López EM, Celikok U, Sengör NS (2021) A dynamical model for the basal ganglia-thalamo-cortical oscillatory activity and its implications in Parkinson's disease. Cogn Neurodyn 15:693–720

Obeso JA, Rodriguez-Oroz M, Marłn C, Alonso P, Zamarbide I, Lanciego JL, Rodriguez-Diaz M (2004) The origin of motor fluctuations in Parkinson's disease: importance of dopaminergic innervation and basal ganglia circuits. Neurology 62:S17–S30

Obeso JA, Marin C, Rodriguez-Oroz C, Blesa J, Benitez-Temiño B, Mena-Segovia J, Rodríguez M, Olanow CW (2008) The basal ganglia in Parkinson's disease: current concepts and unexplained observations. Ann Neurol 64:S30–S46

Oorschot DE (1996) Total number of neurons in the neostriatal, pallidal, subthalamic, and substantia nigral nuclei of the rat basal ganglia: a stereological study using the cavalieri and optical disector methods. J Comp Neurol 366:580–599

Park MR, Falls WM, Kitai ST (1982) An intracellular HRP study of the rat globus pallidus. I. Responses and light microscopic analysis. J Comp Neurol 211:284–294

Paulsen JS, Long JD, Johnson HJ, Aylward EH, Ross CA, Williams JK, Nance MA, Erwin CJ, Westervelt HJ, Harrington DL, Bockholt HJ, Zhang Y, McCusker EA, Chiu EM, Panegyres PK; PREDICT-HD Investigators and Coordinators of the Huntington Study Group (2014) Clinical and biomarker changes in premanifest Huntington disease show trial feasibility: a decade of the PREDICT-HD study. Front Aging Neurosci 6:78

Plotkin JL, Surmeier DJ (2015) Corticostriatal synaptic adaptations in Huntington's disease. Curr Opin Neurobiol 33:53–62

Reed JL, Qi HZ, Zhou Z, Bernard MR, Burish MJ, Bonds A, Kaas JH (2010) Response properties of neurons in primary somatosensory cortex of owl monkeys reflect widespread spatiotemporal integration. J Neurophysiol 103:2139–2157

Reiner A, Albin RL, Anderson KD, D'Amato CJ, Penney JB, Young AB (1988) Differential loss of striatal projection neurons in Huntington disease. Proc Natl Acad Sci U S A 85:5733–5737

Richards C, Shiroyama T, Kitai S (1997) Electrophysiological and immunocytochemical characterization of GABA and dopamine neurons in the substantia nigra of the rat. Neurosci 80:545–557

Richfield EK, Maguire-Zeiss KA, Vonkeman HE, Voorn P (1995) Preferential loss of preproenkephalin versus preprotachykinin neurons from the striatum of Huntington's disease patients. Ann Neurol 38:852–861

Rojas NG, Cesarini ME, Peker G, Da Prat GA, Etcheverry JL, Gatto E (2022) Review of Huntington's disease: from basics to advances in diagnosis and treatment. J Neurol Res 12:93–113

Ross CA, Tabrizi SJ (2011) Huntington's disease: from molecular pathogenesis to clinical treatment. Lancet Neurol 10:83–98

Rubin JE (2017) Computational models of basal ganglia dysfunction: the dynamics is in the details. Curr Opin Neurobiol 46:127–135

Sadek AR, Magill PJ, Bolam JP (2007) A single-cell analysis of intrinsic connectivity in the rat globus pallidus. J Neurosci 27:6352–6362

Sen-Bhattacharya B, James S, Rhodes O, Sugiarto I, Rowley A, Stokes AB, Gurney K, Furber SB (2018) Building a spiking neural network model of the basal ganglia on SpiNNaker. IEEE Trans Cogn Develop Syst 10:823–836

Sharma M, Deogaonkar M (2015) Deep brain stimulation in Huntington's disease: assessment of potential targets. J Clin Neurosci 22:812–817

Shen KZ, Johnson SW (2006) Subthalamic stimulation evokes complex EPSCs in the rat substantia nigra pars reticulata in vitro. J Physiol 573:697–709

Shen Y, Campbell RE, Côté DC, Paquet ME (2020) Challenges for therapeutic applications of opsin-based optogenetic tools in humans. Front Neural Circuits 14:41

Shimazaki H, Shinomoto S (2010) Kernel bandwidth optimization in spike rate estimation. J Comput Neurosci 29:171–182

Squire LR, Bloom FE, McConnell SK, Roberts JL, Spitzer NC, Zigmond MJ (2003) Fundamental Neuroscience. Academic Press, New York

Tecuapetla F, Matias S, Dugue GP, Mainen ZF, Costa RM (2014) Balanced activity in basal ganglia projection pathways is critical for contraversive movements. Nat Commun 5:4315

Tesler F, Tort-Colet N, Depannemaecker D, Carlu M, Destexhe A (2022) Mean-field based framework for forward modeling of LFP and MEG signals. Front Comput Neurosci 16:968278

Thibeault CM, Srinivasa N (2013) Using a hybrid neuron in physiologically inspired models of the basal ganglia. Front Comput Neurosci 7:88

Tomkins A, Vasilaki E, Beste C, Gurney K, Humphries MD (2014) Transient and steady-state selection in the striatal microcircuit. Front Comput Neurosci 7:192

Turner RS, DeLong MR (2000) Corticostriatal activity in primary motor cortex of the macaque. J Neurosci 20:7096–7108

Walker FO (2007) Huntington's disease. Lancet 369:218–228

Wang XJ (2010) Neurophysiological and computational principles of cortical rhythms in cognition. Physiol Rev 90:1195–1268

Wang X, Yu Y, Han F, Wang Q (2022) Beta-band bursting activity in computational model of heterogeneous external globus pallidus circuits. Commun Nonlinear Sci Numer Simul 110:106388

Wojtecki L, Groiss SJ, Hartmann CJ, Elben S, Omlor S, Schnitzler A, Vesper J (2016) Deep brain stimulation in Huntington's disease - Preliminary evidence on pathophysiology, efficacy and safety. Brain Sci 6:38

Wolf JA, Moyer JT, Lazarewicz MT, Contreras D, Benoit-Marand M, O'Donnell P, Finkel LH (2005) NMDA/AMPA ratio impacts state transitions and entrainment to oscillations in a computational model of the nucleus accumbens medium spiny projection neuron. J Neurosci 25:9080–9095

Yin L, Han F, Yu Y, Wang Q (2023) A computational network dynamical modeling for abnormal oscillation and deep brain stimulation control of obsessive-compulsive disorder. Cogn Neurodyn 17:1167–1184

Yu Y, Han F, Wang Q, Wang Q (2022) Model-based optogenetic stimulation to regulate beta oscillations in Parkinsonian neural networks. Cogn Neurodyn 16:667–681

Zheng T, Wilson CJ (2002) Corticostriatal combinatorics: the implications of corticostriatal axonal arborizations. J Neurophysiol 87:1007–1017